Journal of Solid State Chemistry **161,** 113–120 (2001)
doi:10.1006/jssc.2001.9296, available online at http://www.idealibrary.com on IDEAL®

Crystal Structure and Magnetic Properties of 6H-Perovskite $Ba_3NdRu_2O_9$

Yoshihiro Doi and Yukio Hinatsu

Division of Chemistry, Graduate School of Science, Hokkaido University, Sapporo 060-0810, Japan

and

Yutaka Shimojo and Yoshinobu Ishii

Japan Atomic Energy Research Institute, Tokai-mura, Ibaraki 319-1195, Japan

Received April 9, 2001; in revised form July 5, 2001; accepted July 12, 2001

Magnetic properties of a quaternary oxide $Ba_3NdRu_2O_9$ are reported. This compound adopts the 6H-perovskite structure with space group $P6_3/mmc$, in which the cation sites within the face-sharing octahedra are occupied by ruthenium ions and those within the corner-sharing octahedra are occupied by neodymium ions. Powder neutron diffraction, powder X-ray diffraction, magnetic susceptibility, magnetization, and specific heat measurements were carried out. It was found that the crystal phase transition and magnetic transition occurred at *ca.* 120 K and 24 K, respectively. The crystal structure below 120 K is monoclinic with space group $C2/c$. Neutron diffraction data collected at 10 K show that $Ba_3NdRu_2O_9$ has a long-range ferromagnetic ordering of Nd^{3+} ions. The ordered magnetic moment of Nd^{3+} ions is 1.65(8) μ_B. The direction of ordered moments is parallel to the *c*-axis.

1. INTRODUCTION

It is well known that perovskite and perovskite-like oxides containing ruthenium ions often exhibit interesting magnetic and electrical properties (1, 2). The perovskite-type oxides have the general formula ABO_3, in which A represents a large transition metal ion and B represents a small one. The B site can accommodate two kinds of metal ions and the general formula of such a compound is given as $A_2BB'O_6$. Recently, the crystal structures and magnetic properties of a series of ordered perovskites A_2LnRuO_6 (A = Sr or Ba; Ln = lanthanide elements) in which the Ln and Ru ions regularly order have been investigated. Battle *et al.* reported that Sr_2ErRuO_6 exhibited an antiferromagnetic transition involving both Ru^{5+} and Er^{3+} ions at *ca.* 40 K, and its magnetic structure was determined by the neutron diffraction measurements (3). We have measured magnetic susceptibilities of Sr_2LnRuO_6 (Ln = Eu–Lu) and found that they show very unique and complex magnetic behavior below *ca.* 40 K (4). In these compounds, most of the magnetic transitions may be due to the magnetic interaction between the Ru^{5+} ([Kr]$4d^3$ electronic structure; [Kr] = krypton core) and Ln^{3+} ([Xe]$4f^n$ electronic structure; [Xe] = xenon core) ions, which is via a superexchange pathway of Ru–O–Ln (the angle is *ca.* 180°).

We turn our attention to the magnetic properties of the ruthenium-based oxides with the 6H-$BaTiO_3$-type structure (5), which have the general formula $Ba_3MRu_2O_9$ ($M = 3d$ transition metals, lanthanide elements, etc.). In many cases, these compounds have a hexagonal unit cell. Two kinds of B site ions, Ru and M, occupy the face-sharing octahedral sites (Ru_2O_9 dimer) and the corner-sharing octahedral ones (MO_6 octahedron), respectively. The superexchange pathways predicted in this structure are Ru–O–Ru (the interaction in the intra dimer; the angle is *ca.* 90°) and Ru–O–M (the angle is *ca.* 180°). The magnetic coupling between Ru ions in the dimer is usually antiferromagnetic and it is strong. Previously, Darriet *et al.* reported that the temperature dependence of magnetic susceptibilities of $Ba_3M^{2+}Ru_2^{5+}O_9$ (M = Mg, Ca, Cd, and Sr) is characteristic of the antiferromagnet, i.e., a broad maximum appears in the susceptibility vs temperature curve at 400–500 K (6). This behavior is explained by the antiferromagnetic Ru^{5+}–Ru^{5+} coupling in the isolated Ru_2O_9 dimer (6, 7). If the M^{2+} ions are magnetic, another magnetic interaction should operate between Ru^{5+} and M^{2+} ions and the long-range magnetic ordering may be observed. In fact, $Ba_3NiRu_2O_9$ and $Ba_3CoRu_2O_9$ show antiferromagnetic transitions (8), and their magnetic structures have been determined by powder neutron diffraction measurements (9).

In the case that the M ions are lanthanide ones, further interesting magnetic behavior due to the interaction between d and f electrons may be observed. Thumm *et al.*

0022-4596/01 $35.00

reported that $Ba_3LnRu_2O_9$ (Ln = Y, La, Nd, Sm–Gd, Dy–Yb) adopted a 6H-$BaTiO_3$-type structure (10, 11). Rath and Müller-Buschbaum measured the magnetic susceptibility of $Ba_3LnRu_2O_9$ (Ln = Gd and Yb) over the temperature range 77–650 K (12), and it shows Curie–Weiss-like behavior. It has been reported that most of the ordered perovskites A_2LnRuO_6 show antiferromagnetic transitions at 25–45 K and that the Ru–O–Ln pathway (the angle is *ca.* 180°) is responsible for the magnetic interactions (3, 4, 13). Therefore, we can expect to observe magnetic cooperative phenomena due to the interaction between d and f electrons in the $Ba_3LnRu_2O_9$ compounds at sufficiently low temperatures.

In this paper, we have focused our attention on a compound $Ba_3NdRu_2O_9$, and performed its magnetic susceptibility, magnetization, and specific heat measurements in the temperature range 1.8–300 K, and its neutron diffraction measurements at 10, 60 and 180 K and room temperature. Their results will be discussed here.

2. EXPERIMENTAL

2.1. Sample Preparation

A polycrystalline sample of $Ba_3NdRu_2O_9$ was prepared by the conventional solid-state reaction. As starting materials, $BaCO_3$, RuO_2, and Nd_2O_3 were used. Before use, Nd_2O_3 was dried in air at 900°C for a day. The samples were weighed in an appropriate metal ratio and well mixed in an agate mortar. The mixtures were pressed into pellets and then calcined at 900°C for 12 h. The calcined materials were fired in air at 1200°C for 12×2 h and at 1300°C for 12×5 h with several interval grindings and pelletings. The heating rate was 100°C/h. The progress of the reaction was monitored by powder X-ray diffraction (XRD) measurements.

A diamagnetic $Ba_3SrNb_2O_9$, which is isomorphous with $Ba_3NdRu_2O_9$, was also prepared. As will be described later, this compound is needed to estimate the lattice contribution of the specific heat to the total specific heat of $Ba_3NdRu_2O_9$. As starting materials, $BaCO_3$, $SrCO_3$, and Nb (metal) were used. The stoichiometric mixtures were calcined in air, first at 950°C for 12×2 h and then at 1350°C for 48 h, and finally, were heated at 1300°C for 48 h in a flow of helium gas. The XRD measurements showed that $Ba_3SrNb_2O_9$ was formed as a single phase and that its crystal structure agreed with a previous report (14).

2.2. X-Ray and Neutron Diffraction Measurements

The powder X-ray diffraction profile at room temperature was measured in the range $10° \le 2\theta \le 120°$ using a 2θ step size of 0.02° with Cu$K\alpha$ radiation on a Rigaku MultiFlex diffractometer. The XRD measurements at 13–200 K were carried out using a Rigaku RINT2200 diffractometer. A sample was cooled by a variable temperature cryostat system, CryoMini (Iwatani Industrial Gases Co.).

Powder neutron diffraction measurements were performed at 10, 60, 180, and 300 K using a high-resolution powder diffractometer (HRPD) (15) at the JRR3-M reactor (Japan Atomic Energy Research Institute), with a Ge(331) monochromator (λ = 1.82268 Å). The collimators used were 6′–20′–6′ and were placed before and after the monochromator, and between the sample and each detector. The set of 64 detectors and collimators, which were placed every 2.5°, rotates around the sample. Crystal and magnetic structures were determined by the Rietveld technique, using the program RIETAN2000 (16).

2.3. Magnetic and Thermal Measurements

The magnetic measurements were carried out using a SQUID magnetometer (Quantum Design, MPMS-5S). The temperature dependence of the magnetic susceptibilities was measured under both zero-field-cooled (ZFC) and field-cooled (FC) conditions in an applied field of 0.1 T over the temperature range 1.8–400 K. The magnetization measurements were performed at 2, 10, 21, and 25 K over the magnetic field $0 \le H \le 5$ T.

The remanent magnetization measurements were also performed. The sample was cooled to 5 K in a zero field. The magnetic field was applied up to 5 T and then reduced to zero, and the magnetization measurements were performed in the temperature range from 5 to 30 K.

Specific heat measurements were performed using a relaxation technique with a commercial heat capacity measurement system (Quantum Design, PPMS model) in the temperature range 1.8–300 K. The sintered sample in the form of a pellet was mounted on a thin alumina plate with grease for better thermal contact.

3. RESULTS AND DISCUSSION

3.1. Crystal Structure of $Ba_3NdRu_2O_9$

3.1.1. Crystal structure at room temperature. Both the X-ray and the neutron diffraction data indicate that $Ba_3NdRu_2O_9$ is formed as a single phase and have a hexagonal symmetry at room temperature. The neutron diffraction profile measured at room temperature is shown in Fig. 1a. The data have been quantitatively analyzed by the Rietveld method in order to refine the crystal structure of this compound. The results show that the crystal structure of $Ba_3NdRu_2O_9$ is the 6H-perovskite structure with space group $P6_3/mmc$ (No. 194). The crystal structure of $Ba_3NdRu_2O_9$ is illustrated in Fig. 2. The structural parameters are summarized in Table 1. This structure is the same as those of the analogous compounds $Ba_3LnRu_2O_9$ (Ln = Y, Gd, and Yb (12); Sm, Dy, and Er (17)). The unit cell parameters, a_{hex} and c_{hex}, are 5.9319(1) and 14.7589(3) Å,

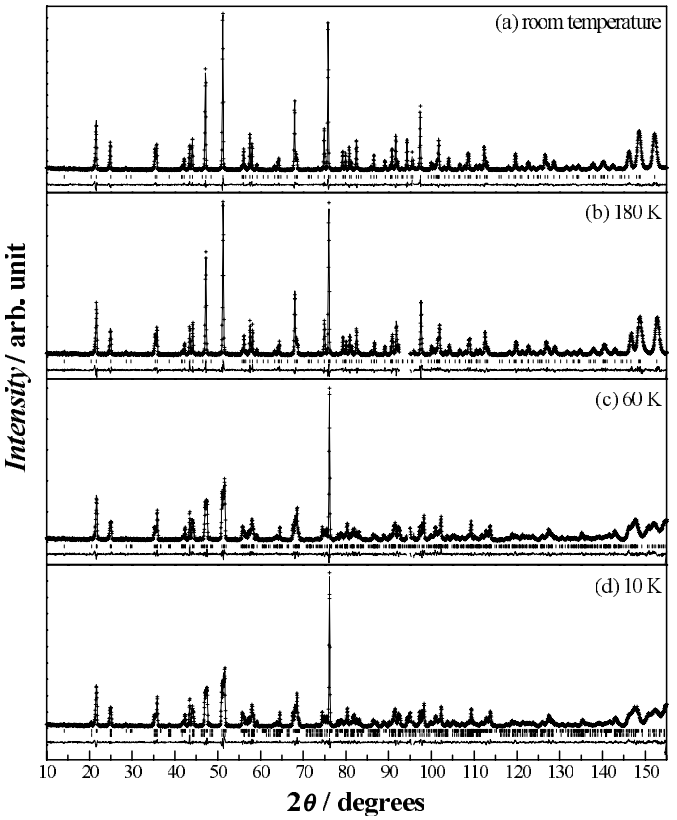

FIG. 1. Powder neutron diffraction profiles for $Ba_3NdRu_2O_9$. The calculated and observed diffraction profiles are shown with the top solid line and cross markers, respectively. The vertical marks in the middle show positions calculated from the nuclear reflections. In (d), the lower vertical marks show the magnetic reflection positions. The bottom trace is a plot of the difference between calculated and observed intensities.

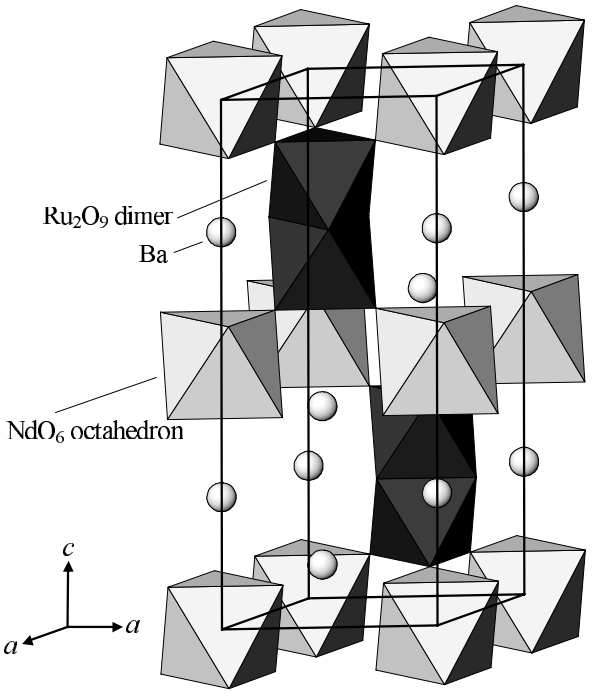

FIG. 2. The crystal structure of $Ba_3NdRu_2O_9$ at room temperature.

respectively, which agree with the lattice parameters reported previously (11). The cation sites within the face-sharing octahedra of this structure are occupied by ruthenium ions and those within the corner-sharing octahedra are occupied by neodymium ions. No evidence of the occurrence of the cation disorder or oxygen defect has been found.

Some selected bond lengths and angles are listed in Table 2. In this structure, the NdO_6 octahedra have six equal Nd–O bond lengths and are regular in shape. In contrast, the RuO_6 octahedra in the Ru_2O_9 dimer are not regular. The Ru–O(1) bond lengths (O(1) atoms are on the shared-face in the Ru_2O_9 dimer) are longer than the Ru–O(2) bond lengths (O(2) atoms are on the top or bottom face of the Ru_2O_9 dimer). The average Ru–O lengths are 1.979(2) Å, and this value is in the middle between 1.997 Å in the $Ru_2^{4+}O_9$ dimer of $Ba_3CeRu_2O_9$ (17) and 1.965 Å in the $Ru_2^{5+}O_9$ dimer of $Ba_3MRu_2O_9$ (M = Zn and Ni) (9). This fact indicates that the average valency of ruthenium ions is + 4.5, as is expected from the trivalent oxidation state of neodymium ions and the stoichiometry in the oxygen content.

3.1.2. Crystal structure at low temperatures. Neutron diffraction measurements were performed at 10, 60, and 180 K to check whether the crystal phase transition occurred or not, and to determine the crystal structures at low temperatures. Their diffraction profiles are shown in Fig. 1, and the results were analyzed by the Rietveld method. The crystal structure at 180 K is the same as that at room temperature (space group $P6_3/mmc$) (see Table 1). The diffraction data collected at 10 and 60 K indicate that the crystal structures at these temperatures have a lower symmetry than that at 180 K. Initially, we attempted to analyze these profiles by assuming a structure model in which the crystal symmetry is orthorhombic with space group $Cmcm$ ($a_{ortho} \approx a_{hex}$, $b_{ortho} \approx \sqrt{3}b_{hex}$, $c_{ortho} \approx c_{hex}$) which is the same as that for $Ba_3CoRu_2O_9$ at 2 K (9, 18). However, this assumption gave an unsatisfactory result. Therefore, we have lowered the symmetry of the crystal structure model from orthorhombic to monoclinic. It has been found that the analysis using a structure model which has a monoclinic symmetry with space group $C2/c$ (No. 15) gives a good agreement with experimental data. The crystal structure of $Ba_3NdRu_2O_9$ at 60 K is illustrated in Fig. 3. The unit cell parameters (a_{mono}, b_{mono}, c_{mono}, and β_{mono}) at 60 K are 5.9173(3), 10.2425(5), 14.7663(9) Å, and 90.819(2)°,

TABLE 1
Structural Parameters for $Ba_3NdRu_2O_9$ (Hexagonal Phase)

Atom	Site	x	y	z	B/Å^2
Space group: $P6_3/mmc$ (No. 194); $z = 2$					
Room temperature					
$a = 5.9319(1)$ Å, $c = 14.7589(3)$ Å, $V = 449.75(2)$ Å^3					
$R_{wp} = 7.65\%$, $R_I = 2.64\%$, $R_F = 1.69\%$, $R_e = 5.82\%$					
Ba(1)	2*b*	0	0	$\frac{1}{4}$	0.34(7)
Ba(2)	4*f*	$\frac{1}{3}$	$\frac{2}{3}$	0.8994(2)	0.86(5)
Nd	2*a*	0	0	0	0.10(5)
Ru	4*f*	$\frac{1}{3}$	$\frac{2}{3}$	0.1645(1)	0.63(3)
O(1)	6*h*	0.4885(2)	0.9769	$\frac{1}{4}$	0.70(3)
O(2)	12*k*	0.1779(2)	0.3557	0.4084(1)	1.04(3)
180 K					
$a = 5.9245(2)$ Å, $c = 14.7643(6)$ Å, $V = 448.79(3)$ Å^3					
$R_{wp} = 11.58\%$, $R_I = 3.80\%$, $R_F = 2.41\%$, $R_e = 9.58\%$					
Ba(1)	2*b*	0	0	$\frac{1}{4}$	0.42(11)
Ba(2)	4*f*	$\frac{1}{3}$	$\frac{2}{3}$	0.8998(3)	0.48(8)
Nd	2*a*	0	0	0	0.31(7)
Ru	4*f*	$\frac{1}{3}$	$\frac{2}{3}$	0.1645(2)	0.41(5)
O(1)	6*h*	0.4881(3)	0.9762	$\frac{1}{4}$	0.51(6)
O(2)	12*k*	0.1787(2)	0.3573	0.4078(1)	0.73(5)

Note. Definitions of reliability factors R_{wp}, R_I, R_F, and R_e are given as follows:

$$R_{wp} = [\sum w(|F_o| - |F_c|)^2 / \sum w|F_o|^2]^{1/2}, \quad R_I = \sum |I_{ko} - I_{kc}| / \sum I_{ko},$$

$$R_F = \sum |I_{ko}^{1/2} - I_{kc}^{1/2}| / \sum I_{ko}^{1/2}, \quad R_e = [(N-p)/\sum_i w_i y_i^2]^{1/2}.$$

respectively. The structural parameters are summarized in Table 3, and the bond lengths and angles are listed in Table 4.

The neutron diffraction profile at 10 K indicates that there exist some magnetic reflection peaks due to a ferromagnetic ordering of Nd^{3+} ions, as will be described later. The crystal and magnetic structures at 10 K have been determined by the Rietveld method. The crystal structure at 10 K has the same symmetry as that at 60 K. The magnetic structure will be discussed in Section 3.2.3.

TABLE 2
Selected Bond Lengths (Å) and Angles (°) for $Ba_3NdRu_2O_9$ (Hexagonal Phase)

	Room temperature	180 K
Nd–O(2) ×6	2.273(1)	2.284(2)
Ru–O(1) ×3	2.033(2)	2.029(3)
–O(2) ×3	1.926(2)	1.912(3)
Ru–O (average)	1.979(2)	1.971(3)
Ru–Ru	2.524(4)	2.525(6)
Ru–O(2)–Nd	177.5(1)	177.3(1)
Ru–O(1)–Ru	76.8(1)	77.0(2)

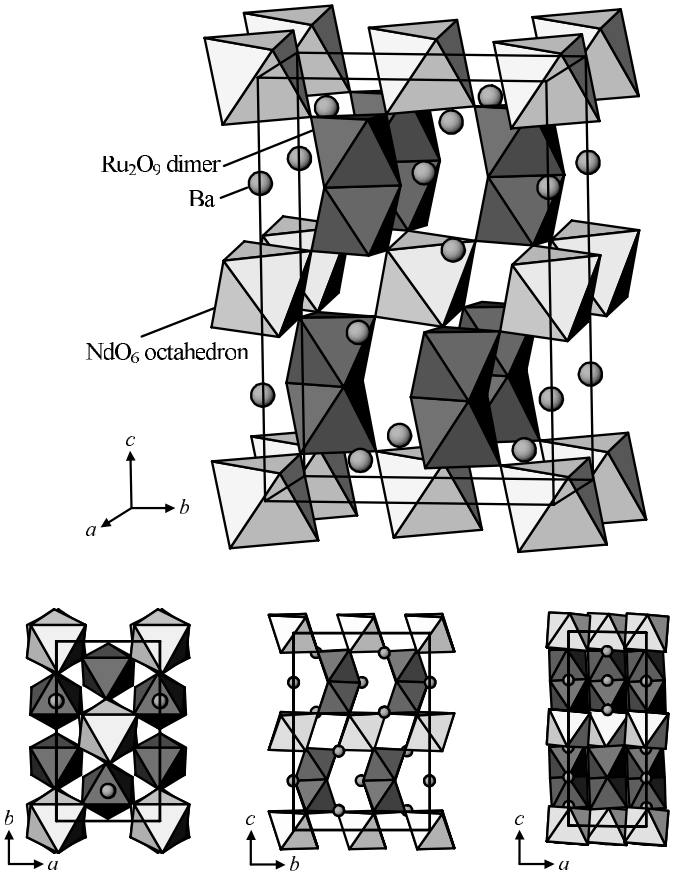

FIG. 3. The crystal structure of $Ba_3NdRu_2O_9$ at 60 K.

Powder X-ray diffraction measurements were also performed in the temperature range of 13 to 200 K. The diffraction profiles collected at 13–110 K are indexed in a monoclinic unit cell ($C2/c$), and those collected at 130–200 K are indexed in a hexagonal unit cell ($P6_3/mmc$). Therefore, it is considered that the structural phase transition occurs around 120 K.

3.2. *Magnetic Properties of $Ba_3NdRu_2O_9$*

3.2.1. Magnetization measurements. The temperature dependence of the magnetic susceptibility (M/H) of $Ba_3NdRu_2O_9$ is plotted in Fig. 4. The magnetic susceptibility shows a rapid increase when the temperature is decreased through 24 K, and the large divergence between the ZFC and FC susceptibilities is found below this temperature. These results indicate that a ferromagnetic or a ferrimagnetic transition has occurred at 24 K. We have already prepared analogous compounds $Ba_3LnRu_2O_9$ (Ln = Y, La, Lu) in which only Ru ions are magnetic, and we have measured their magnetic susceptibilities (19). They show antiferromagnetic transitions below 15 K. Hence, the Nd ions should contribute to the magnetic transition of

TABLE 3
Structural Parameters for $Ba_3NdRu_2O_9$ (Monoclinic Phase)

Atom	Site	x	y	z	B/Å^2
space group: $C2/c$ (No. 15); $z = 4$					
60 K					
$a = 5.9173(3)$ Å, $b = 10.2425(5)$ Å, $c = 14.7663(9)$ Å					
$\beta = 90.819(2)^\circ$, $V = 894.86(8)$ Å^3					
$R_{wp} = 11.73\%$, $R_I = 3.48\%$, $R_F = 1.94\%$, $R_e = 9.61\%$					
Ba(1)	4*e*	0	− 0.0030(12)	$\frac{1}{4}$	0.10(7)
Ba(2)	8*f*	0.0038(9)	0.3313(8)	0.0989(3)	0.10(7)
Nd	4*a*	0	0	0	0.19(9)
Ru	8*f*	− 0.0060(6)	0.3317(7)	0.8360(3)	0.31(7)
O(1)	4*e*	0	0.5147(9)	$\frac{1}{4}$	0.30(10)
O(2)	8*f*	0.2654(13)	0.2417(7)	0.2446(5)	0.40(10)
O(3)	8*f*	0.0188(12)	0.8210(6)	0.0926(4)	0.29(13)
O(4)	8*f*	0.2835(11)	0.0920(7)	0.0830(4)	0.57(11)
O(5)	8*f*	0.7536(12)	0.0891(6)	0.0988(4)	0.45(12)
10 K					
$a = 5.9138(3)$ Å, $b = 10.2352(4)$ Å, $c = 14.7633(8)$ Å					
$\beta = 90.847(2)^\circ$, $V = 893.51(7)$ Å^3					
$R_{wp} = 10.00\%$, $R_I = 2.00\%$, $R_F = 1.16\%$, $R_e = 7.09\%$					
Ba(1)	4*e*	0	− 0.0031(10)	$\frac{1}{4}$	0.04(6)
Ba(2)	8*f*	0.0037(7)	0.3323(7)	0.0995(3)	0.04(6)
Nd	4*a*	0	0	0	0.20(7)
Ru	8*f*	− 0.0075(5)	0.3326(6)	0.8353(2)	0.44(6)
O(1)	4*e*	0	0.5131(7)	$\frac{1}{4}$	0.20(8)
O(2)	8*f*	0.2625(11)	0.2426(6)	0.2440(4)	0.63(8)
O(3)	8*f*	0.0212(10)	0.8219(5)	0.0927(4)	0.25(11)
O(4)	8*f*	0.2829(9)	0.0913(6)	0.0828(4)	0.75(9)
O(5)	8*f*	0.7506(10)	0.0906(6)	0.0975(4)	0.53(11)
Magnetic moment of Nd: 1.65(8) μ_B					
Direction of moment: [001]					

TABLE 4
Selected Bond Lengths (Å) and Angles (°) for $Ba_3NdRu_2O_9$ (Monoclinic Phase)

	60 K	10 K
Nd–O(3) ×2	2.290(6)	2.282(5)
–O(4) ×2	2.267(6)	2.260(6)
–O(5) ×2	2.269(6)	2.274(5)
Nd–O (average)	2.276(6)	2.272(5)
Ru–O(1)	2.023(9)	2.021(7)
–O(2)	2.014(8)	2.028(7)
–O(2)	2.042(8)	2.051(7)
–O(3)	1.888(8)	1.907(7)
–O(4)	1.931(7)	1.946(6)
–O(5)	1.942(7)	1.926(6)
Ru–O (average)	1.973(8)	1.980(7)
Ru–Ru	2.542(8)	2.522(7)
Ru–O(3)–Nd ×2	174.3(4)	173.7(3)
Ru–O(4)–Nd ×2	174.3(4)	174.2(3)
Ru–O(5)–Nd ×2	169.4(4)	171.3(4)
Ru–O–Nd (average)	172.7(4)	173.1(3)
Ru–O(1)–Ru	77.9(4)	77.2(4)
Ru–O(2)–Ru ×2	77.6(3)	76.4(3)
Ru–O–Ru (average)	77.7(4)	76.7(3)

$Ba_3NdRu_2O_9$ observed at 24 K. The temperature dependence of the inverse susceptibility (H/M) is shown in an inset graph in Fig. 4. A linear relationship between the inverse susceptibility vs temperature is observed above 120 K. Below this temperature, the susceptibility deviates from this relationship, which is due to the structural phase transition. The higher temperature data ($T > 200$ K) are fitted using the Curie–Weiss law. The obtained effective magnetic moment and Weiss constant are 5.82(3) μ_B and − 85(3) K, respectively.

The temperature dependence of the remanent magnetization is plotted in Fig. 5. The remanent magnetization is constant (*ca.* 1.05 μ_B) below 15 K and decreases with increasing temperature between 15 and 24 K and is zero above 24 K. The field dependence of the magnetization at 2, 10, 21, and 25 K is shown in Fig. 6. Data collected below 21 K show a hysteresis loop, which means that there exists a ferromagnetic moment.

3.2.2. Specific heat measurements. Figure 7 shows the variation of the specific heat for $Ba_3NdRu_2O_9$ as a function of temperature. Two anomalies have been observed at 17 and 24 K. The λ-type anomaly at 24 K corresponds to the magnetic transition found in the magnetic susceptibility. No anomaly corresponding to the structural phase transition at *ca.* 120 K has been found in this measurement.

The specific heat data for $Ba_3SrNb_2O_9$ are also plotted in Fig. 7. The crystal structure of this compound is analogous to that of $Ba_3NdRu_2O_9$ at room temperature (space group

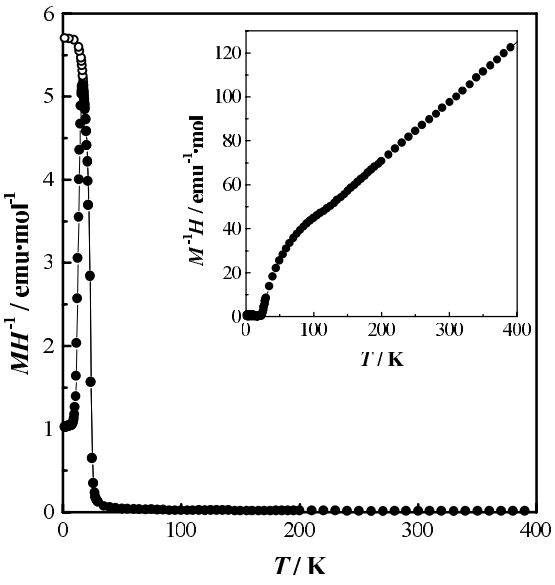

FIG. 4. Magnetic susceptibilities (M/H) of $Ba_3NdRu_2O_9$. The filled and open symbols show the ZFC and FC susceptibilities, respectively. The applied field is 0.1 T. Inset shows the inverse susceptibility.

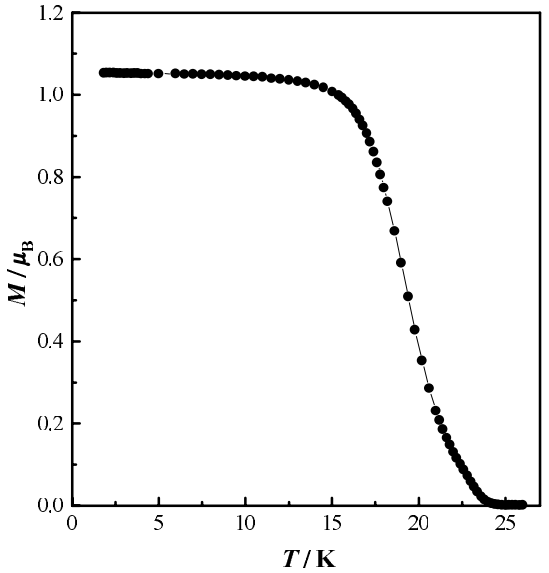

FIG. 5. Temperature dependence of the remanent magnetization of $Ba_3NdRu_2O_9$.

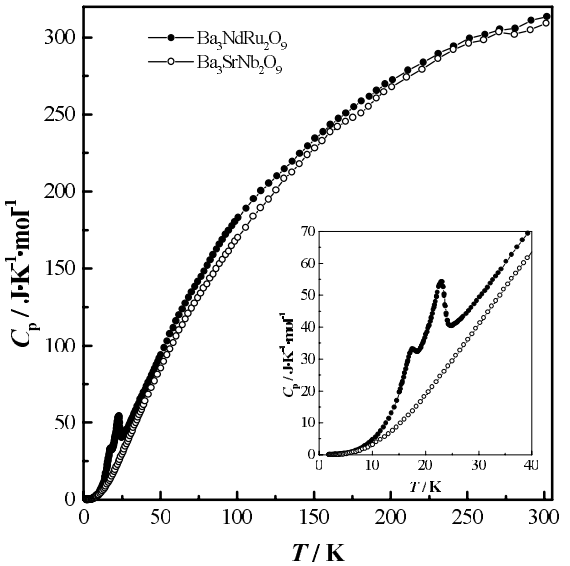

FIG. 7. Temperature dependences of the specific heat for $Ba_3NdRu_2O_9$ and $Ba_3SrNb_2O_9$.

$P6_3/mmc$), and it has no magnetic ions. If we assume that the electronic and lattice contributions to the specific heat are equal between $Ba_3NdRu_2O_9$ and $Ba_3SrNb_2O_9$, the magnetic specific heat for $Ba_3NdRu_2O_9$ is obtained by subtracting the specific heat of $Ba_3SrNb_2O_9$ from that of $Ba_3NdRu_2O_9$.

The temperature dependence of the magnetic specific heat divided by temperature (C_M/T) and of the magnetic entropy (S_M) is shown in Fig. 8. The magnetic entropy change (ΔS_M) between 1.8 and 24 K is *ca.* 11.1 J/mol K. This value is the sum of the entropy changes for two anomalies at 17 and 24 K. It seems that the entropy changes of these anomalies are equal; in that case, each entropy change is very close to $R \ln W = R \ln 2 = 5.76$ J/mol K (R is a molar gas constant). Above 24 K, the entropy increases with temperature. This may indicate the occurrence of a short-range magnetic ordering.

3.2.3. Magnetic structure at 10 *K.* As has been mentioned in Section 3.1.2, some magnetic reflection peaks are

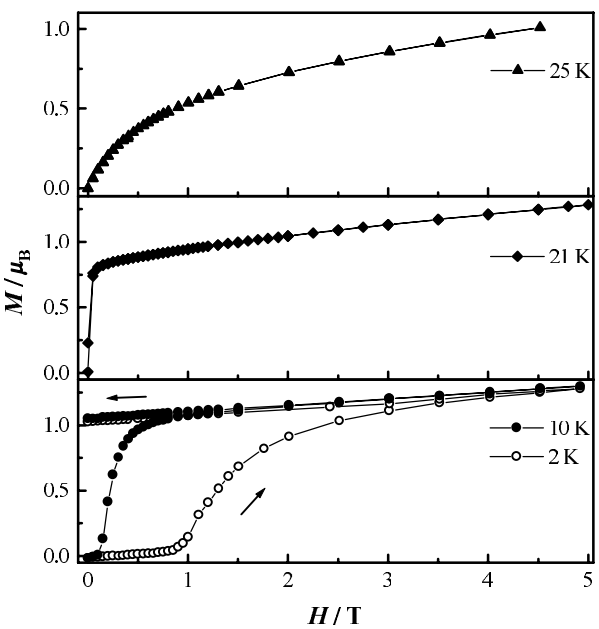

FIG. 6. Field dependence of the magnetization of $Ba_3NdRu_2O_9$.

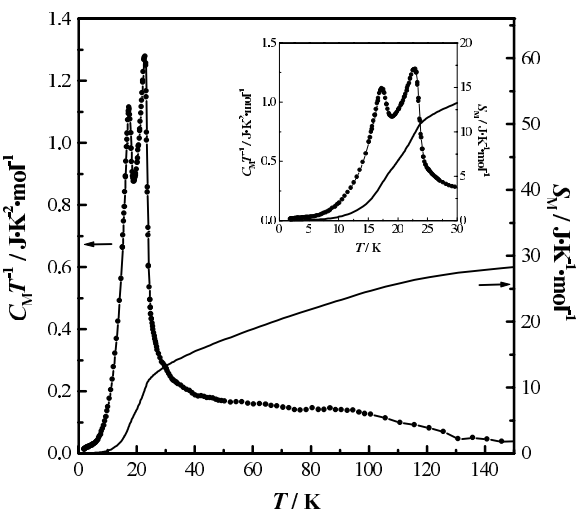

FIG. 8. The magnetic specific heat divided by temperature (C_M/T) and magnetic entropy (S_M) of $Ba_3NdRu_2O_9$.

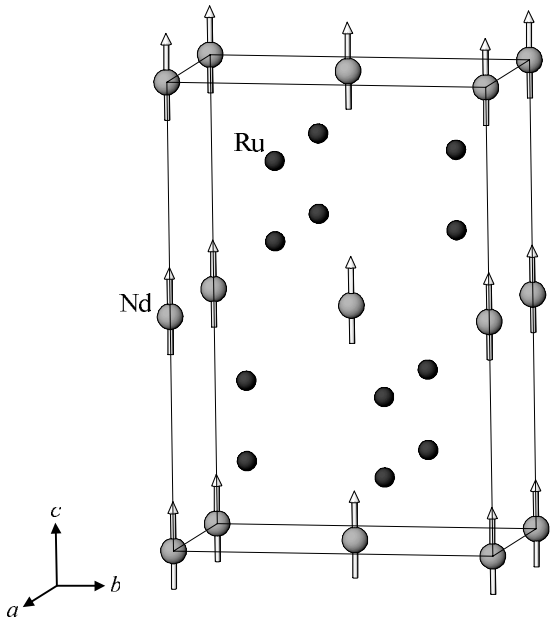

FIG. 9. The magnetic structure of $Ba_3NdRu_2O_9$ at 10 K. Diamagnetic ions are omitted. The arrows indicate the direction of the magnetic moments.

observed in the neutron diffraction data collected at 10 K. The positions of the magnetic diffraction lines are in accordance with those of the nuclear ones. Our Rietveld analysis determines the magnetic structure of $Ba_3NdRu_2O_9$, which is illustrated in Fig. 9. In this magnetic structure, the magnetic moments of Nd^{3+} ions order ferromagnetically and are aligned along the *c*-axis. The ordered magnetic moment is 1.65(8) μ_B/Nd^{3+} ion. The ordered moments of Ru ions have not been determined in this study and we will discuss this in the following section.

3.2.4. Discussion on the magnetic properties of $Ba_3NdRu_2O_9$. The results of the magnetization, specific heat, and neutron diffraction measurements for $Ba_3NdRu_2O_9$ show that a ferromagnetic ordering of Nd^{3+} ions occurs at 24 K. $Ba_3NdRu_2O_9$ is considered to be nonmetallic because it shows the magnetic behavior of the localized electrons and because the analogous compounds $Ba_3MRu_2O_9$ (M = Fe, Co, Ni, Cu, and In) are semiconductors below room temperature (20). The neutron diffraction data at 10 K show that the crystal structure of $Ba_3NdRu_2O_9$ is distorted monoclinically and that the magnetic structure is described by a ferromagnetic ordering of Nd^{3+} ions; the ordered magnetic moment is 1.65(8) μ_B/Nd^{3+} ion and the direction of ordered moments is parallel to the *c*-axis. The magnetic entropy change of the magnetic transition at 24 K is close to R ln 2. We predict that this magnetic entropy is due to the ground Kramers' doublet of Nd^{3+} ions.

In contrast, the ordered moments of Ru ions have not been determined from the present neutron diffraction data. However, we believe that Ru ions are not in the paramagnetic state at low temperatures. If the Ru ions are paramagnetic down to 10 K, the magnetic transition found at 24 K should be due to only the ordering of Nd ions. We consider that this transition temperature is exceptionally high, because it is known that the magnetic interaction between the *f* electrons is generally very weak compared with that between the *d* electrons, and because the main pathway of the magnetic exchange interaction between Nd ions is a long superexchange pathway of Nd–O–O–Nd. The strong antiferromagnetic coupling between Ru^{5+} ions in the Ru_2O_9 dimer has been found in the analogous compounds such as $Ba_3MRu_2O_9$ (M = Mg, Ca, Sr, and Cd) (6, 7), and the magnetic susceptibility for $Ba_3YRu_2O_9$ does not obey the Curie–Weiss law between 77 and 650 K (12). Our preliminary susceptibility measurements show that magnetic moments of Ru ions in $Ba_3LnRu_2O_9$ (Ln = Y, La, Lu) are coupled antiferromagnetically in the Ru_2O_9 dimer (19). Taking into account that the average valency of ruthenium ions is +4.5, there may exist $Ru^{4+}Ru^{5+}O_9$ dimers. Each dimer has a total spin $S_{dimer} = 1/2$. If the magnetic ordering between dimers occurs at low temperatures, the entropy change $\Delta S_M = R \ln (2S_{dimer} + 1) = R \ln 2$ should be observed. The entropy change for an anomaly at 17 K, which is close to R ln 2, may be due to the magnetic ordering of these Ru_2O_9 dimers. Our failure to detect the ordered moments of Ru ions may be due to the short-range ordering and/or the unsaturation of magnetic moments of Ru ions. In order to clarify the magnetic properties of $Ru_2^{4.5+}O_9$ dimers, further studies on the other $Ba_3LnRu_2O_9$ (Ln = lanthanides) are needed.

ACKNOWLEDGMENTS

This work was supported by The Iwatani Naoji Foundation's Research Grant. Y. D. thanks the Research Fellowships of the Japan Society for the Promotion Science for Young Scientists.

REFERENCES

1. A. Callaghan, C. W. Moeller, and R. Ward, *Inorg. Chem.* **5,** 1572–1576 (1966).
2. Y. Maeno, H. Hashimoto, K. Yoshida, S. Nishizaki, T. Fujita, J. G. Bednorz, and F. Lichtenberg, *Nature* **372,** 532–534 (1994).
3. P. D. Battle and C. W. Jones, *J. Solid State Chem.* **90,** 302–312 (1991).
4. Y. Doi and Y. Hinatsu, *J. Phys.: Condens. Mater* **11,** 4813–4820 (1999).
5. R. D. Burbank and H. T. Evans, *Acta Crystallogr.* **1,** 330–336 (1948).
6. J. Darriet, M. Drillon, G. Villeneuve, and P. Hagenmuller, *J. Solid State Chem.* **19,** 213–220 (1976).
7. J. Darriet, J. L. Soubeyroux, and A. P. Murani, *J. Phys. Chem. Solids* **44,** No.3, 269–272 (1983).

8. R. C. Byrne and C. W. Moeller, *J. Solid State Chem.* **2,** 228–235 (1970).
9. P. Lightfoot and P. D. Battle, *J. Solid State Chem.* **89,** 174–183 (1990).
10. I. Thumm, U. Treiber, and S. Kemmler-Sack, *Z. Anorg. Allg. Chem.* **477,** 161–166 (1981).
11. U. Treiber, S. Kemmler-Sack, A. Ehmann, H.-U. Schaller, E. Dürrschmidt, I. Thumm, and H. Bader, *Z. Anorg. Allg. Chem.* **481,** 143–152 (1981).
12. M. Rath and H. Müller-Buschbaum, *J. Alloys Compd.* **210,** 119–123 (1994).
13. Y. Doi, Y. Hinatsu, K. Oikawa, Y. Shimojo, and Y. Morii, *J. Mater. Chem.* **10,** 797–800 (2000).
14. S. Kemmler-Sack, I. Thumm, and M. Herrmann, *Z. Anorg. Allg. Chem.* **479,** 177–183 (1981).
15. Y. Morii, *J. Cryst. Soc. Jpn.* **34,** 62–69 (1992).
16. F. Izumi and T. Ikeda, *Mater. Sci. Forum* **321–324**, 198–203 (2000).
17. H. Müller-Buschbaum and B. Mertens, *Z. Naturforsch. b* **51,** 79–84 (1996).
18. J. T. Rijssenbeek, Q. Huang, R. W. Erwin, H. W. Zandbergen, and R. J. Cava, *J. Solid State Chem.* **146,** 65–72 (1999).
19. Y. Doi and Y. Hinatsu, unpublished results.
20. J. T. Rijssenbeek, P. Matl, B. Batlogg, N. P. Ong, and R. J. Cava, *Phys. Rev. B* **58,** No.16, 10315–10318 (1998).